Suppression of modulation-induced polarization error in splice-less open-loop fiber optic gyroscope

Lin Chen（陈 琳）[1], Peitong He（何沛彤）[2]，Biqiang Jiang（姜碧强）[1*]，and Jianlin Zhao（赵建林）[1]**

[1] Key Laboratory of Light Field Manipulation and Information Acquisition, and Shaanxi Key Laboratory of Optical Information Technology, School of Physical Science and Technology, Northwestern Polytechnical University, Xi'an 710129, China

[2] Zhejiang Lab, Hangzhou ,311100, China

*Corresponding author: bqjiang@nwpu.edu.cn; ** corresponding author: jlzhao@nwpu.edu.cn

Received Month X, XXXX; accepted Month X, XXXX; posted online Month X, XXXX

The suppression of polarization crosstalk in PZT phase modulators as a key error source has been challenging for open-loop fiber optic gyroscopes (FOGs). We developed a polarization-diversity optical frequency domain reflectometry (OFDR) to measure distributed modulation polarization error in the modulator. The error contributes 8×10^{-6} rad to FOG's bias instability. By using a UV-fabricated in-fiber λ/4 waveplate and polarization-mode converter with fiber taper technology, the modulation error has been suppressed by 15 dB in assembled FOGs. This approach reduced error with temperature from 25 °/h to 0.7 °/h, meeting the requirements of control-level gyroscopes with bias errors less than 1 °/h.

Keywords*:* Fiber optic gyroscope (FOG), inline waveplate, optical frequency domain reflectometry (OFDR), polarization-mode converter.
DOI: 10.3788/COLXXXXXX.XXXXXX.

1. Introduction

Fiber optic gyroscopes (FOGs) are widely used in motion sensing and inertial navigation technologies to accurately measure angular velocity [1]. They can be classified into open-loop and closed-loop FOGs [2]. Open-loop FOGs have slightly lower accuracy than closed-loop ones, but their cost advantage is favored by cost-sensitive industries such as autopilot and robot control [3,4].

Open-loop FOGs use Lead zirconate titanate (PZT) modulator, which is only 1/100th the price of the lithium niobate electro-optic modulator used in closed-loop FOGs [5]. However, piezoelectric modulation via squeezing and stretching optical fiber wound on a ceramic, can induce polarization crosstalk and modulation birefringence, causing phase errors [6,7]. The typical co-frequency and in-phase error resulting from the PZT phase modulation has a value approximately ranging from 10^{-5} to 10^{-6} rad. This error significantly deteriorates the accuracy of rotational phase demodulation, and it is thus a primary error source in open-loop FOGs [8]. In addition, there are few optical suppression methods available to mitigate modulation parasitic errors, and traditional polarization measurement methods, such as the polarization-extinction ratio (PER), are not even adequate for assessing such minute levels of polarization crosstalk. Current research primarily focuses on the system-level analysis and algorithm-based compensation of PZT-modulated FOGs [9,10], but they all fall short in achieving high precision in FOG development. To address these issues, we developed a polarization-diversity coherent optical frequency domain reflectometry (OFDR) with high-polarization-extinction light launching capability to measure the distributed modulation polarization error. For the higher sensitivity of the FOG, 40 μm ultra-fine diameter polarization-maintaining (PM) fiber is employed to increase the length of coiled fiber under a limited volume. However, a corresponding challenge arises due to the unavailability of reliable fusion splicing approach for this fiber. To overcome this limitation, we proposed and demonstrated two approaches in a splice-less FOG optical configuration, including an inline UV-induced waveplate approach and an inline polarization mode converter (PMC), to suppress the modulation polarization error. By combining these approaches, our experimental results show that the optimized FOG achieved a polarization error suppression of over 15 dB and reduced the full-temperature peak-to-peak gyro error from 25 °/h to 0.7 °/h, which meets the requirements for a control-level gyroscope with 1 °/h bias stability.

2. Theoretical analysis and measurement

The gyroscope used in this work is based on a spliceless all-fiber FOG architecture [11] with all of its fiber-optical components sequentially fabricated on a 40 μm PM fiber. As shown in Fig. 1, the light source is a superluminescent diode at a center wavelength of 830 nm[2], in order to gain more sensitivity in a compact form factor. The fused biconical tapered couplers are used for the splitting and combining light. The polarizer for polarization filtering is an in-line 45° tilted fiber grating (TFG) with a PER of more than 35 dB [12,13]. The fiber coil with a diameter of 30 mm, acts as the rotation sensitive component with a total length of 150 m. The modulator which is used for generating sinusoidal phase modulation is a PZT ring with a diameter of 10 mm. It has a 1m-long fiber wound at a tension of 0.06 N, and its modulation frequency is of about 120 kHz.

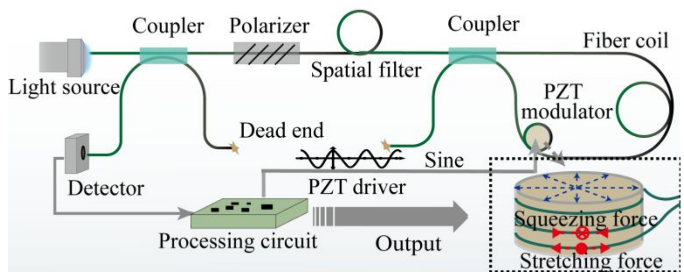

Fig. 1. Schematic structure of a spliceless open-loop FOG.

Using the Jones Matrix method to analyze the optical path of the gyro, we can express the polarization error, E_r, resulting from polarization crosstalk induced by the phase modulation as [8]

$$\begin{aligned}E_r = {} & hl\Delta\phi\cos(\omega\tau/2)\cos(2\alpha)\sin(2\pi l/l_b)\left[1+J_0(\phi_m)-J_2(\phi_m)\right]\sin(\omega t)\\ & +\Delta\phi_m\cos(\omega\tau/2)\cos(2\alpha)\sin(2\pi l/l_b)\left[1+J_0(\phi_m)+J_2(\phi_m)\right]\cos(\omega t)\end{aligned} \quad (1)$$

where, h is the polarization crosstalk of the modulated fiber, l is length of fiber wound on the PZT modulator, $\Delta\phi$ is the birefringent phase difference caused by the modulation, ω is the modulation circular frequency, τ is the transit time of light in the fiber, α is the polarization angle, i.e., $\alpha = \arctan(E_x/E_y)$, where E_x and E_y are the amplitudes in x and y polarization axes, l_b is the fiber beat length (about 3 mm at room temperature), and $\Delta\phi_m$ is the induced phase difference between the two principal axes of PM fiber during the phase modulation process. In this study, $\Delta\phi_m \approx 10^{-4}$. The demodulated output of the open-loop FOG is $I = I_0 J_1(\phi_m)\sin\phi_s \sin(\omega t)$, where ϕ_s is the phase shift to be measured, which is caused by the rotation of the FOG, and $J_n(\phi_m)$ is the nth order Bessel function of the first kind of the modulation depth ϕ_m [14].

From (1), the modulation polarization error can be divided by two parts of the quadrature part with the $\cos(\omega t)$ term and the in-phase part with the $\sin(\omega t)$ term according to the demodulated signal. The quadrature part can be suppressed to 10^{-7} rad by precise phase-locking and can be neglected compared with the in-phase error. Hence, our work mainly focuses on the study of suppressing in-phase error. When the modulation length, frequency, and transit time are determined, the in-phase modulation polarization error is primarily determined by the polarization crosstalk, the birefringence phase difference, and the amplitude ratio of the light in the two principal axes. The influence of modulation-related error of gyroscope is estimated through theoretical analysis and experiments below.

The phase change of the modulator $\delta\phi$ is realized by periodically stretching and squeezing the optical fiber fixed on the ceramic outer circle, which can be estimated as $\delta\phi \approx 0.78\beta l\varepsilon$, where β is the propagation constant of the fiber polarization mode and ε is the applied strain on the fiber [16]. The modulation depth of open-loop FOG with sinusoidal modulation ϕ_m is calculated by $\phi_m = 2\delta\phi\sin(\omega\tau/2)$. When $\phi_m = 1.84$ rad, the gyroscope operates at its highest sensitivity. In this scenario, the maximum strain of the fiber is approximately 4.5×10^{-7}. The optical fiber is wound on the outer circle of the piezoelectric ceramic under significant tension, and the angle between the principal axis of the optical fiber and the deformation direction of the piezoelectric ceramic is θ. As shown in Fig. 2(b), fiber bending, together with stretching and squeezing in the modulation process, generates a parasitic birefringence inevitably at the same frequency as the modulation. The propagation constant difference due to birefringence, $\Delta\beta$, can be estimated by the following formula [9]

$$\Delta\beta = \pi n^3 (P_{12} - P_{11})(1+\nu)\left(\frac{2-3\nu}{1-\nu}\right)\frac{a}{R}\varepsilon/\lambda(\cos\theta - \sin\theta) \qquad (2)$$

where, n is the refractive index of the fiber, a is the cladding radius, R is the radius of PZT, λ is the operating wavelength, p_{11} and p_{12} are the elastic-optic coefficients of the fiber, and ν is Poisson's ratio. During the drawing process, PM fiber's polarization principal axis rotates slowly, causing $\Delta\beta$ to change gradually along its propagation axis. With the parameters used, the birefringent phase difference caused by modulation is approximately 7×10^{-3} rad. In addition, the large initial tension used in winding the piezoelectric ceramic modulator and the transverse force exerted on the fiber by the piezoelectric deformation will increase the polarization crosstalk significantly. This crosstalk, h, can be estimated by the following equations [15]

$$h = (1/16 l_b)\sin^2(2\chi)\left[1 - \cos(2\pi l_b K/\lambda)\right]^2 \qquad (3)$$

wherein,

$$\chi = \arctan\left[\frac{\varepsilon\left(0.04 f\nu + 4\varepsilon Y\nu\pi a^2\right)(p_{11} - p_{12})\sin 2\theta/\pi l_b}{\Delta n - \varepsilon\left(0.04 f\nu + 4\varepsilon Y\nu\pi a^2\right)(p_{11} - p_{12})\cos 2\theta/\pi l_b}\right] \qquad (4)$$

$$K = \begin{bmatrix} \Delta n^2 + \varepsilon^2 (p_{11} - p_{12})^2 (0.04 f\nu/\pi a + 4\varepsilon\nu Ya)^2 \\ -2\varepsilon(p_{11} - p_{12})\Delta n(0.04 f\nu/\pi a + 4\varepsilon\nu Ya)\cos(2\theta) \end{bmatrix}^{1/2} \qquad (5)$$

where Δn is the birefringence of the fiber, Y is the Young's modulus, f is the winding tension of the PZT modulator. Based on Eqs. (3) to (5), when the ϕ_m is 1.84 rad, the average value of polarization crosstalk is about −30 dB/m. Accurate measurement of polarization crosstalk and validating theoretical calculations serve as the foundation for further research on error suppression methods. Traditional optical time-domain distributed measurement methods often have spatial resolutions exceeding 0.2 m. However, the length of the coiled fiber on the PZT modulator is only about 1 m. To accurately measure the distributed polarization crosstalk when the modulator is in action, an OFDR system is developed to measure Rayleigh scattering from two polarization principal axes[16-18]. The in-house OFDR system achieves a remarkable sensitivity of up to −140 dB and a spatial resolution of 8 μm, comparable to commercial systems' performance in the telecom bands. Its schematic diagram is shown in Fig. 2(a).

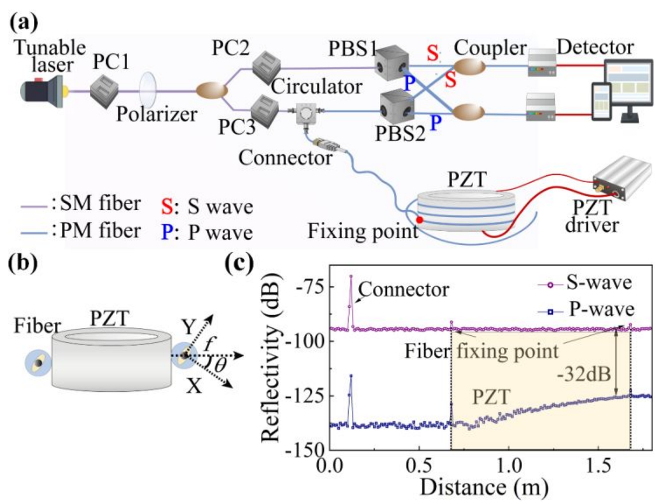

Fig. 2. (a) Schematic diagram of OFDR, (b) force of PZT on optical fiber, and (c) measurement results of fiber polarization crosstalk.

The output of a mode-hop-free wavelength-swept laser with a wavelength range of 815 nm to 845 nm is linearly polarized using an in-house developed 45° TFG with a PER exceeding 50 dB. It is then divided into two parts through a coupler. 50% of the light is kept as the local oscillator light, while the other 50% is sent, *via* an optical circulator, to the measurement path that contains the fiber wound around the piezoelectric ceramic. The polarization state of the light launched into the PM fiber on the PZT modulator is controlled by a polarization controller. In the experiment, it is aligned with the fast axis of the PM fiber. At the far end of the fiber wound on the PZT modulator, the measured PER exceeds 40 dB. The OFDR measurement is employed to confirm that the intensity difference of the Rayleigh backscattered light between the S-wave and P-wave states also surpasses 40 dB, which is expected because of the superior polarization crosstalk performance (−45 dB/m) of the PM fiber used for the FOG. The Rayleigh scattered light on the optical fiber returns to the main path through the circulator, which is then split into two principal polarization states (S-wave and P-wave) via a polarization beam splitter (PBS). Subsequently, they are mixed with two copies of the local oscillator reference light, obtained via a PBS (the upper one in Fig. 2(a), to form a frequency domain interference signal). The crosstalk of the polarization state of the fiber on the modulator can then be obtained via inverse Fourier Transform of the record interference signal. This OFDR has a spatial resolution of 8 μm and a sensitivity of −140 dB. When the modulation depth is 1.84 rad, the obtained experimental results are shown in Fig. 2(c). The Rayleigh scattering feature is clearly shown on the OFDR trace for S-wave and P-wave. Initially, the scattered S-wave is much larger than P-wave, which agrees with the fact that the light is launched into the fast axis. After the fiber fixing point on the PZT ceramic, the light starts to couple into the slow-axis, and the coupled power increases monotonically with the distance. When the light exits the modulator (the fiber fixing point at the distance end), the crosstalk reaches about −32 dB, which moderately agrees with our theoretical analysis above.

For the traditional polarization-maintaining open-loop FOG, the linearly polarized light filtered by the polarizer is aligned with the principal axis of the fiber, and the polarization is maintained along the whole optical path, i.e., $\alpha = 0$. Substituting the analyzed and measured polarization crosstalk, birefringent propagation constant, and the gyroscope's design parameters into Eq. (1), we can obtain a modulation polarization error approximately 8×10^{-6} rad. The corresponding gyroscope bias error reaches 15 °/h [11], which is larger than the requirements of < 1 °/h for the widely used gyroscope in motion gesture control.

3. Methods and verifications

From Eq. (1), as the polarization angle α approaches 45°, i.e., the light amplitude of x and y polarization axes are equal, the polarization error reaches a minimum value. It can be obtained by inserting a λ/4 waveplate following the polarizer with the waveplate axis aligned 45° to that of the polarizer [19]. Because there is no reliable splicing method for our 40 μm ultra-fine PM fiber, both the polarizer and the waveplate are required to be fabricated in the form of fiber in-line. Fortunately, the fiber optic industry has already developed versatile ultraviolet (UV) inscription technology for in-line fiber optic devices. The employed polarizer is based on a 45° TFG [20,21]. The waveplate can be fabricated using the UV inscription method as shown in Fig. 3(a).

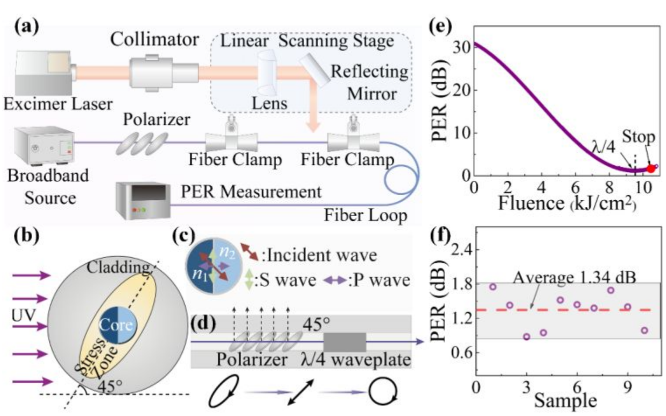

Fig. 3. Inscription of fiber in-line waveplate: (a) inscription setup; (b) inscription principle; (c) mechanism resulting birefringence; (d) polarization conversion; (e) PER evolution; (f) PER distribution of 10 samples.

A 248 nm KrF excimer laser with a single pulse energy density of 20 mJ/cm^2 is used for waveplate inscription. A cylindrical lens is used to focus the light into the fiber core. The cylindrical lens and reflecting mirror are mounted on a linear scanning stage, enabling the scanning of the UV beam along the fiber. The scanning speed is 50 μm/s, and the required length of the waveplate is precisely controlled by adjusting the scanning time. The fiber is hydrogen loaded with 100 atmospheres at 85°C for 48 h for sensitization treatment [22]. The optical fiber is rotated under the microscope to align its principal axis at 45° to the incident direction of UV light. The refractive index of optical fiber increases with the absorption of UV light [23-25]. Since the front part of the optical fiber facing the incoming UV beam absorbs more light, the corresponding UV-induced refractive index change is higher than that of the back part of the fiber, as shown in Fig. 3(b), which in turn causes birefringence as shown in Fig. 3(c) [23,24]. The irradiation fluence and the waveplate length control the phase retardation of this UV-induced fiber in-line birefringence waveplate, which is monitored in-situ as the waveplate is being fabricated. As shown in Figure 3(d), without the need to cut the fiber for fabricating individual devices, a broadband light source is first coupled into the ultra-fine fiber, and then it is filtered by a 45° TFG polarizer fabricated before the waveplate, resulting in highly linearly polarized output light with a PER of at least 35 dB. Since the principal axis of the waveplate is 45° to the principal axis of the fiber, as its phase delay grows, the polarization state will change from linear polarization to elliptical polarization and to circular polarization when the phase retardation is $\pi/2$. This kind of polarization change can be monitored using the PER value of the output light, and the result is shown in Fig. 3(e) for a 20 mm long waveplate. With the increasing UV fluence and thus phase delay, the initial high PER drops gradually to almost zero, indicating the conversion of linear polarized light to nearly perfect circularly polarized light.

The inscribed λ/4 waveplate needs to be annealed at 100 °C for 24 h for long-term stability [26]. Such practice usually results in approximately 10% birefringence degradation. Therefore, in a practical inscription, the waveplate needs to be over-inscribed by about 10% after the PER reaches a minimum value near zero. However, the degradation mentioned above is related to various factors such as fiber characteristics and hydrogen-loading sensitization. Considering the large dispersiveness of process control and the axis alignment error, the PER after annealing could be controlled within 1.8 dB in our work as shown in Fig. 3(f) for 10 samples, indicating the technical soundness of our *in-situ* monitoring method. Using these samples' average PER of 1.34 dB, α is calculated to be 4.4° away from the optimal value of 45°, and in this case, the modulation polarization error could be suppressed by 8 dB. It is worth noting that, from Eq. (1), the in-line inscription of λ/4 waveplate could also suppress the quadrature error by the same proportion. However, the modulation polarization error should be suppressed to more than 12 dB, and the gyro accuracy can reach 1 °/h. It is therefore necessary to combine other technical solutions to suppress the error.

The above analysis suggests that the polarization error cannot be reduced to a value less than 1 °/h using waveplate alone. An in-line polarization mode converter is proposed to be combined with the waveplate to further suppress the error. Modulation polarization error is proportional to the induced birefringence phase difference. If the polarization modes are exchanged at the midpoint of the optical fiber, and the birefringence generated by modulation is equal at two locations with the same distance from the midpoint, then

$$\Delta\phi = \int_0^{l/2} \Delta\beta(z)\mathrm{d}z - \int_{l/2}^{l} \Delta\beta(z)\mathrm{d}z = 0 \quad (6)$$

where, z is the location of the fiber. This means the phase retardation due to birefringence effectively cancels out. However, traditional PZT ceramic modulators use a unipolar spiral fiber winding form [11], and the midpoint is in the center of the piezoelectric ceramic. It is impossible to put a PMC there. As shown in Fig. 4(a), we resort to a bipolar symmetrical winding form, of which the fiber midpoint is placed away outside of the ceramic, and the lead fiber of the PMC located at the midpoint is wound in the vicinity of the piezoelectric ceramic to ensure that the modulation birefringence at the symmetrical position is the same.

A traditional method of making a PMC is to cleave an optical fiber to obtain two cleaved fibers and rotate these two fibers' axis so that one fiber's fast axis is aligned to the other one's slow axis and then splice them together. However, our fiber cannot be spliced, so we developed a modified taper technology to fabricate such a polarization mode converter. As shown in Figs. 4(b) and 4(c), a 2mm-long segment of optical fiber is subjected to a hydrogen-oxygen flame fusion process and slowly stretched to a length of 8 mm. This process results in the formation of an adiabatic double taper structure with a parabolic shape. The diameter of the tapered region is approximately 6 μm. A 90° rotation is located at the narrowest zone of the taper, effectively achieving the desired polarization mode conversion. The tapered PMC is packaged and protected in a quartz tube[27].

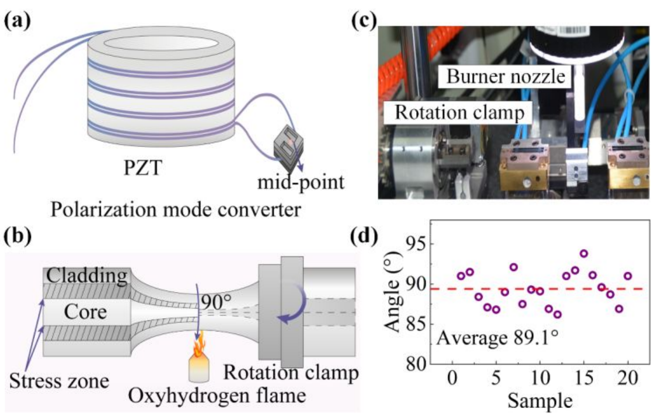

Fig. 4. Fabrication of in-line PMC: (a) bipolar symmetrically wound PZT modulator; (b) schematic of PMC fabrication processing; (c) photo of our fabrication setup; (d) measurement result of 20 samples.

By utilizing the fabrication methods described above, a total of 20 PMCs are produced, and the polarization angle variation during fabrication is assessed using a PER meter, as shown in Figs. 4(d). Statistical analysis reveals that the polarization angle variation is 86°±4°, and the deviation from 90° could be attributed to inadvertent rotation during the cooling process of the optical fiber. It is estimated that the modulation polarization error can be suppressed by an average of 11 dB and a minimum of 6 dB.

The enhanced FOG configuration, incorporating both a waveplate and a PMC, is depicted in Fig. 5(a). These devices will be added sequentially in the experiment for comparative testing. The modulation polarization error is proportional to $\sin(2\pi l/l_b)$, where l represents the fiber length and l_b represents the beat length. For stress birefringence fibers, the beat length is proportional to temperature[28]. Consequently, the modulation polarization error exhibits quasi-periodic sinusoidal fluctuation characteristics with temperature. Suppression of modulation polarization error is evaluated by analyzing the amplitude variation of bias with temperature fluctuation, with results presented in Fig. 5(b).

The test results reveal that the traditional open-loop FOG suffers from a significant modulation polarization error. The peak-to-peak temperature-dependent fluctuation is approximately 25 °/h. However, by incorporating an in-line λ/4 waveplate, the modulation polarization error suppression is about 7.1 dB, which is consistent with our analysis above. Subsequently, both an in-line λ/4 waveplate and an in-line PMC are introduced simultaneously in the open-loop FOG. The bias caused by the modulation polarization error with temperature fluctuation is buried in the gyroscope's noise. The peak-peak value is only 0.7 °/h, and the additional suppression is better than 8.4 dB. The combined suppression from the waveplate and the PMC is better than 15 dB, which successfully fulfills the accuracy requirements with a bias error of less than 1 °/h. Allan variance and gyro dynamic characteristics have also been tested as shown in Fig. 5(c). The result shows that the gyro bias instability which can be calculated by dividing the bottom of the curve by 0.664 reaches 0.1 °/h, which meets the requirements of control-level applications.

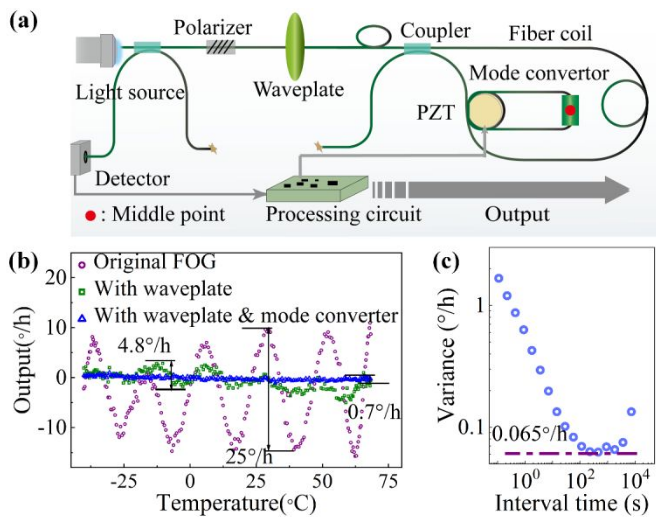

Fig. 5. Enhanced FOG: (a) FOG configuration; (b) comparison of test results with waveplete and PMC added; (c) Allan variance.

4. Conclusion

Polarization crosstalk in the fiber wound on the PZT ceramic modulator is carefully characterized both theoretically and experimentally with self-developed OFDR. A new scheme of open-loop FOG is proposed to overcome the polarization modulation error due to the polarization crosstalk in the modulator. The corresponding critical components under the new scheme, in-line λ/4 waveplate, bipolar symmetric wound PZT modulator, and PMC, are introduced and discussed. Our experimental investigations suggest that under the proposed scheme with practical components fabricated in-house, the polarization modulation error can be significantly reduced by more than 15 dB. The open-loop FOG can achieve a bias error of less than 1 °/h. The findings may open the door to cost-effective FOG, with a wide application scope, including but not limited to motion sensing, gesture control, and inertial navigation.

Acknowledgement

This work was financially supported by the National Natural Science Foundation of China (No. 61975166).

References

1. V. M. N. Passaro, A. Cuccovillo, L. Vaiani, M. De Carlo, and C. E. Campanella, "Gyroscope technology and applications: a review in the industrial perspective," Sensors **17**, 2284 (2017).
2. E. Udd and M. J. F. Digonnet, "Design and development of fiber optic gyroscopes," (2019). **SPIE proceedings.**
3. H. C. Lefèvre, "The fiber-optic gyroscope: Challenges to become the ultimate rotation-sensing technology," Opt. Fiber Technol. **19**, 6 (2013).
4. K. Shang, M. Lei, Q. Xiang, Y. Na, and L. Zhang, "Tactical-grade interferometric fiber optic gyroscope based on an integrated optical chip," Opt. Commun. **485**, 126729 (2021).
5. K Shang, M. Lei, Q. Xiang, Y. Na, L. Zhang, and H. Yu, "Near-navigation-grade interferometric fiber optic gyroscope with an integrated optical chip," Chin. Opt. Lett. **18**, 120601 (2020).
6. M. Skalský, Z. Havránek, and J. Fialka, "Efficient modulation and processing method for closed-loop fiber optic gyroscope with piezoelectric modulator," Sensors **19**, 1710 (2019).
7. K. Shang, M. Lei, H. Li, T. Zhang, X. Yu, Q. Xiang, Y. Na, and L. Zhang, "Ultra-small interferometric fiber optic gyroscope with an integrated optical chip," Chin. Opt. Lett. **20**, 040601 (2022).
8. B. Szafraniec, and J. Blake, "Polarization modulation errors in all-fiber depolarized gyroscopes," J. Lightwave Technol. **12**, 9 (1994).
9. H. J. Jeong, J. H. Kim, H. W. Lee, and B. Y. Kim, "Birefringence modulation in fiber-optic phase modulators," Opt. Lett. **19**, 18 (1994).
10. P. Li, Y. Li, F. Chen, C. Peng, and Z. Li, "Two-Port Noise Suppression in Dual-Polarization Interferometric Fiber-Optic Gyroscope," IEEE Photonics Journal **11**, 2 (2019).
11. R. A. Bergh, H. C. Lefevre, and H. J. Shaw, "All-single-mode fiber-optic gyroscope with long-term stability," Opt. Lett. **6**, 10 (1981).
12. L. Chen, Y. Mao, B. Jiang, and J. Zhao, "Tilted fiber grating polarizer in a 40μm polarization-maintaining fiber," Appl. Opt. **62**, 3 (2023).
13. B. Jiang, X. Zhang, A. Li, Y. Hou, Z. Hao, X. Gan, and J. Zhao, "Electrically induced dynamic Fano-like resonance in a graphene-coated fiber grating," Photon. Res. **10**, 5 (2022).
14. Q. Wang, C. Yang, X. Wang, and Z. Wang, "All-digital signal-processing open-loop fiber-optic gyroscope with enlarged dynamic range," Opt. Lett. **38**, 24 (2013).
15. J. N. Chamoun, and M. J. F. Digonnet, "Noise and bias error due to polarization coupling in a fiber optic gyroscope," J. Lightwave Technol. **33**, 13 (2015).
16. L. Huang, X. Fan, and Z. He, "Scanning-free hybrid Rayleigh–Brillouin distributed fiber-optic sensing system," Opt. Lett. **48**, 17 (2023).
17. Z. Yu, Q. Zhuang, Y. Lin, Y. Lin, C. Lin, B. Rang, Y. Yuan, J. Yang, K. Wen, P. Xu, Y. Wang, and Y. Qin, "Optical frequency domain polarimetry for distributed polarization crosstalk measurement beyond a 110 dB dynamic range," Opt. Lett. **47**, 16 (2022).
18. F. Meng, W. Zhang, X. Liu, F. Liu, and X. Zhou, "Comparative analysis of temporal-spatial and time-frequency features for pattern recognition of φ-OTDR," Chin. Opt. Lett. **21**, 040601 (2023).
19. Q. Song, B. Ye, X. Xiao, C. Huang, C. Mou, Z. Yan, and L. Zhang, "Theoretical and experimental analysis of second order Bragg resonance of 45° TFG and its fiber laser application," Chin. Opt. Lett. **20**, 012201 (2022).
20. B. Jiang, Y. Hou, J. Wu, Y. Ma, X. Gan, and J. Zhao, "In-fiber photoelectric device based on graphene-coated tilted fiber grating," Opto-Electronic Science **2**, 6 (2023).
21. L. Chen, Y. Mao, P. He, H. Wang, B. Jiang, and J. Zhao, "Compact and high-reliability fiber-optic open-loop gyroscope enabled by an in-fiber polarizer," Opt. Express **31**, 3 (2023).
22. B. Jiang, Z. Bi, Z. Hao, Q. Yuan, D. Feng, K. Zhou, L. Zhang, X. Gan, and J. Zhao, "Graphene oxide-deposited tilted fiber grating for ultrafast humidity sensing and human breath monitoring," Sens. Actuators B Chem. **293**, 336 (2019).
23. B. Jiang, Y. Hou, H. Wang, X. Gan, A. Li, Z. Hao, K. Zhou, L. Zhang, and J. Zhao, "Few-layer graphene integrated tilted fiber grating for all-optical switching," J. Lightwave Technol. **39**, 5 (2021).
24. J. P. Mueller, K. Leosson, and F. Capasso, "Ultracompact metasurface in-line polarimeter," Optica **3**, 42 (2016).
25. K. Ozga, "UV-laser induced birefringence in olygoetheracrylate photopolymers," Opt Laser Technol. **98**, 404 (2018).
26. N. Zhong, M. Zhao, Q. Liao, X. Zhu, Y. Li, and Z. Xiong, "Effect of heat treatments on the performance of polymer optical fiber sensor," Opt. Express **24**, 12 (2016).
27. D. Mao, Z. He, H. Lu, M. Li, W. Zhang, X. Cui, B. Jiang, and J. Zhao, "All-fiber radially/azimuthally polarized lasers based on mode coupling of tapered fibers," Opt. Lett. **43**, 7 (2018).
28. Z. Xu, X. Li, Y. Hong, P. Liu, H. Yang, and W. Ling, "Temperature dependence of beat-length and confinement loss in an air-core photonic band-gap fiber," Opt. Commun. **366**, 38 (2016).